

As-Plausible-As-Possible: Plausibility-Aware Mesh Deformation Using 2D Diffusion Priors

Anonymous CVPR submission

Paper ID 15

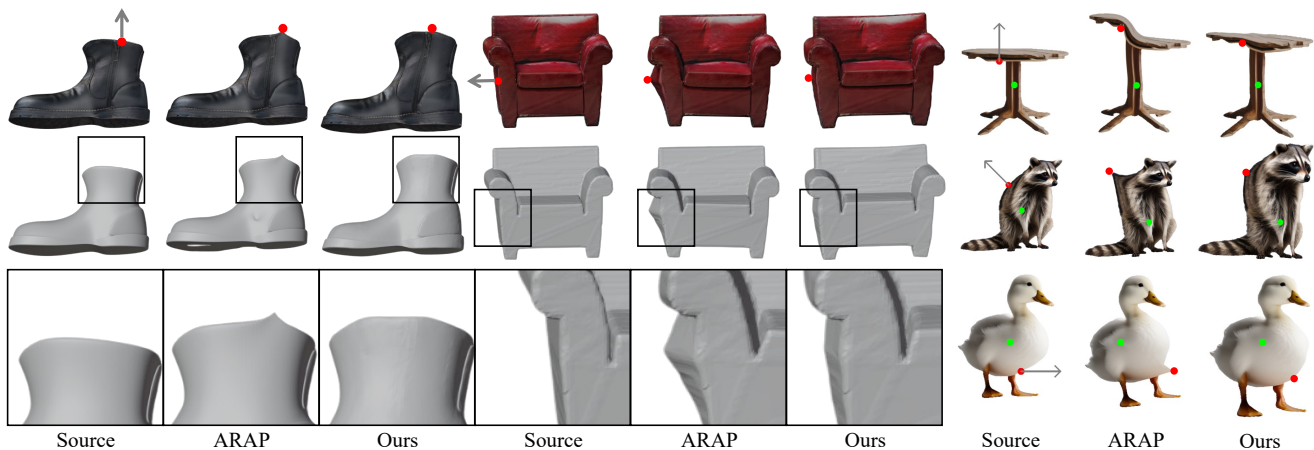


Figure 1. APAP, our novel shape deformation method, enables plausibility-aware mesh deformation and preservation of fine details of the original mesh offering an interface that alters geometry by directly displacing a handle (*red*) along a direction (*gray*). The improvement achieved by leveraging a diffusion prior is illustrated by the smooth geometry near the handle in the armchair example (the middle column).

Abstract

We present *As-Plausible-as-Possible (APAP) mesh deformation technique that leverages 2D diffusion priors to preserve the plausibility of a mesh under user-controlled deformation. Our framework uses per-face Jacobians to represent mesh deformations, where mesh vertex coordinates are computed via a differentiable Poisson Solve. The deformed mesh is rendered, and the resulting 2D image is used in the Score Distillation Sampling (SDS) process, which enables extracting meaningful plausibility priors from a pretrained 2D diffusion model. To better preserve the identity of the edited mesh, we fine-tune our 2D diffusion model with LoRA. Gradients extracted by SDS and a user-prescribed handle displacement are then backpropagated to the per-face Jacobians, and we use iterative gradient descent to compute the final deformation that balances between the user edit and the output plausibility. We evaluate our method with 2D and 3D meshes and demonstrate qualitative and quantitative improvements when using plausibility priors over geometry-preservation or distortion-minimization priors used by previous techniques.*

1. Introduction

For 2D and 3D content, mesh is the most prevalent representation, thanks to its efficiency in storage, simplicity in rendering and also compatibility in common graphics pipelines, versatility in diverse applications such as design, physical simulation, and 3D printing, and flexibility in terms of decomposing geometry and appearance information, with widespread adoption in the industry.

For the creation of 2D and 3D meshes, recent breakthroughs in generative models [29, 35, 39, 46, 47, 49, 53, 56] have demonstrated significant advances. These breakthroughs enable users to easily generate content from a text prompt [35, 39, 47, 53, 56], or from photos [41, 47]. However, visual content creation typically involves numerous editing processes, deforming the content to satisfy users' desires through interactions such as mouse clicks and drags. Facilitating such interactive editing has remained relatively underexplored in the context of recent generative techniques.

Mesh deformation is a subject that has been researched for decades in computer graphics. Over time, researchers have established well-defined methodologies, characteriz-

ing mesh deformation as an optimization problem that aims to preserve specific geometric properties, such as the Mesh Laplacian [32, 33, 51], local rigidity [16, 50], and mesh surface Jacobians [2, 11], while satisfying given constraints. To facilitate user interaction, these methodologies have been extended to introduce specific user-interactive deformation handles, such as keypoints [18, 26, 55], cage mesh [21, 23, 24, 31, 57, 62], and skeleton [4, 60, 61], with the blending functions defined based on the preservation of geometric properties.

Despite the widespread use of classical mesh deformation methods, they often fail to meet users’ needs because they do not incorporate the perceptual plausibility of the outputs. For example, as illustrated in Fig. 1, when a user intends to drag a point on the top of a table image, the classical deformation technique may introduce unnatural bending instead of lifting the tabletop. This limitation arises because deformation techniques solely based on geometric properties do not incorporate such semantic and perceptual priors, resulting in the mesh editing process becoming more tedious and time-consuming.

Recent learning-based mesh deformation techniques [2, 21, 26, 34, 52, 60, 62] have attempted to address this problem in a data-driven way. However, they are also limited by relying on the existence of certain variations in the training data. Even recent large-scale 3D datasets [6–8, 59] have not reached the scale that covers all possible visual content users might intend to create.

To this end, we introduce our novel mesh deformation framework, dubbed APAP (As-Plausible-As-Possible), which exploits 2D image priors from a diffusion model pretrained on an Internet-scale image dataset to enhance the plausibility of deformed 2D and 3D meshes while preserving the geometric priors of the given shape. Recently, score distillation sampling (SDS) [39] has demonstrated great success in generating plausible 2D and 3D content, such as NeRF [22, 27, 65] and vector images [17, 20], using the distilled 2D image priors from a diffusion model. We incorporate these diffusion-model-based 2D priors into the optimization-based deformation framework, achieving the best synergy between geometry-based optimization and distilled-prior-based optimization.

To achieve this optimal synergy between geometric and perceptual priors within a unified framework, we introduce an alternative optimization approach. At each step, we first update the Jacobian of each mesh face using the SDS loss and user-provided constraints. Subsequently, the mesh vertex positions are recalculated by solving Poisson’s equation with the updated face Jacobians. The direct application of the 2D diffusion prior via SDS, however, tends to compromise the identity of the given objects—an essential aspect in deformation. We thus enhance the identity awareness of the diffusion prior by finetuning it with the provided source im-

age. The model is integrated into our two-stage pipeline that initiates deformation without the perceptual prior (SDS) and refines it with SDS and the given constraints afterward to create deformations that adhere to user-defined editing instructions while remaining visually plausible.

In experiments, we examine APAP using APAP-BENCH consisting of 3D and 2D triangular meshes and editing instructions. The proposed method produces plausible deformations of 3D meshes compared to its baseline [50] based exclusively on a geometric prior. Evaluation in the task of 2D mesh editing further verifies the effectiveness of APAP as illustrated by the highest k -NN GIQA score [12] in quantitative analysis, and the higher preference over the baseline in a user study.

2. Related Work

2.1. Geometric Mesh Deformation

Mesh deformation has been one of the central problems in geometry processing and is thus addressed by a wide range of techniques. Cage-based methods [23, 24, 31, 57] let users alter meshes by manipulating cages enclosing them, calculating a point inside as a weighted sum of cage vertices. Skeleton-based approaches [4, 58, 60, 61] offer animation control by mapping surface points to underlying joints and bones, ideal for animating human/animal-like figures. Unlike the previous techniques that require the manual cage or skeleton construction, biharmonic coordinates-based methods [18, 55] automate establishing mappings from control points to vertices by formulating optimization problems. Other types of works instead allow users to manipulate shapes via direct vertex displacement while imposing constraints on local surface geometry, including rigidity [16, 50] and Laplacian smoothness [32, 33, 51]. Such hand-crafted deformation priors often lack consideration of visual plausibility, necessitating careful control point placement and iterative manual refinement to achieve satisfactory results.

2.2. Data-Driven Mesh Deformation

Data-driven approaches to mesh deformation [2, 21, 26, 34, 52, 60, 62] learn from shape collections, utilizing neural networks to infer parameters for classical deformation techniques, such as cage vertex coordinates and displacements [62], keypoints [21, 26, 55], subspaces of keypoint arrangements [34], differential coordinates [2], etc. However, these methods assume the availability of large-scale category-specific shape collection [21, 26, 55, 60, 62] or require dense correspondences between them [2, 52], limiting their applicability to new, out-of-sample shapes. We instead propose to directly mine deformation priors from pretrained diffusion models. Leveraging a generic (category-agnostic) image generative model trained on an Internet-scale image

dataset, we devise a method that easily generalizes to novel 2D and 3D shapes while lifting the requirement for shape collections.

2.3. Pretrained 2D Priors for Shape Manipulation

Image analysis [40] and generation [3, 30, 43, 63] techniques can serve as effective visual priors for image editing tasks [5, 14, 48, 54, 64]. In addition, recent work [10, 44] and their adaption [9], enable personalized image generation and editing by learning a text embedding [10] or fine-tuning additional parameters, such as LoRA [15] to preserve and replicate the identities of given exemplars during editing. One interesting work is DragDiffusion [48], akin to DragGAN [37], which introduces a drag-based user interface for image editing through the manipulation of latent representations. However, it is not extendable to the deformation of parametric images, such as 2D meshes, and also 3D shapes. Another interesting line of works [11, 25, 36] extends the idea further to manipulate shapes by propagating image-based gradients to the underlying shape representations. They maximize CLIP [40] similarity between the renderings and text prompts to either add geometric textures [36], jointly update both vertices and texture [25], or deform a shape parameterized by per-triangle Jacobians [11]. In contrast to such text-driven editing techniques, we build on Score Distillation Sampling (SDS) [39] to enable direct manipulation of shapes via handle displacement, ensuring visual plausibility. While the technique is prevalent in various problems ranging from text-to-3D [35, 39, 47, 53, 56], image editing [13] and neural field editing [65], it has not been adopted for shape deformation.

3. Method

We present **APAP**, a novel handle-based mesh deformation framework capable of producing visually plausible deformations of either 2D or 3D triangular meshes. To achieve this goal, we integrate powerful 2D diffusion priors into a learnable Jacobian field representation of shapes.

We emphasize that leveraging 2D priors, such as latent diffusion models (LDMs) [43] trained on large-scale datasets [45], for shape deformation poses challenges that require meticulous design choices. The following sections will delve into the details of shape representation (Sec. 3.1) and diffusion prior (Sec. 3.2), offering a rationale for the design decisions underpinning our framework (Sec. 3.3).

3.1. Representing Shapes as Jacobian Fields

Let $\mathcal{M}_0 = (\mathbf{V}_0, \mathbf{F}_0)$ denote a source mesh to be deformed, represented by vertices $\mathbf{V}_0 \in \mathbb{R}^{V \times 3}$ and faces $\mathbf{F}_0 \in \mathbb{R}^{F \times 3}$. Users are allowed to select a set of vertices used as movable handles designated by an indicator matrix $\mathbf{K}_h \in \{0, 1\}^{V_h \times V}$. We also require users to select a set of anchors, represented as another indicator ma-

trix $\mathbf{K}_a \in \{0, 1\}^{V_a \times V}$, to avoid trivial solutions (i.e., global translations). Then, the handle and anchor vertices become $\mathbf{V}_h = \mathbf{K}_h \mathbf{V}_0$ and $\mathbf{V}_a = \mathbf{K}_a \mathbf{V}_0$.

Our framework also expects a set of vectors $\mathbf{D}_h \in \mathbb{R}^{V_h \times 3}$ that indicate the directions along which the handles will be displaced. Furthermore, we let $\mathbf{T}_h = \mathbf{V}_h + \mathbf{D}_h$ and $\mathbf{T}_a = \mathbf{V}_a$ denote the target positions of the user-specified handles and anchors, respectively.

In this work, we employ a Jacobian field $\mathbf{J}_0 = \{\mathbf{J}_{0,f} | f \in \mathbf{F}_0\}$, a dual representation of \mathcal{M}_0 , defined as a set of per-face Jacobians $\mathbf{J}_{0,f} \in \mathbb{R}^{3 \times 3}$ where

$$\mathbf{J}_{0,f} = \nabla_f \mathbf{V}_0, \quad (1)$$

and ∇_f is the gradient operator of triangle f .

Conversely, we compute a set of *deformed* vertices \mathbf{V}^* from a given Jacobian field \mathbf{J} by solving a Poisson’s equation

$$\mathbf{V}^* = \arg \min_{\mathbf{V}} \|\mathbf{L}\mathbf{V} - \nabla^T \mathcal{A}\mathbf{J}\|^2, \quad (2)$$

where ∇ is a stack of per-face gradient operators, $\mathcal{A} \in \mathbb{R}^{3F \times 3F}$ is the mass matrix and $\mathbf{L} \in \mathbb{R}^{V \times V}$ is the cotangent Laplacian of \mathcal{M}_0 , respectively. Since \mathbf{L} is rank-deficient, the solution of Eqn. 2 cannot be uniquely determined unless we impose constraints. We thus consider a constrained optimization problem

$$\mathbf{V}^* = \arg \min_{\mathbf{V}} \|\mathbf{L}\mathbf{V} - \nabla^T \mathcal{A}\mathbf{J}\|^2 + \lambda \|\mathbf{K}_a \mathbf{V} - \mathbf{T}_a\|^2, \quad (3)$$

where $\lambda \in \mathbb{R}^+$ is a weight for the constraint term. Note that we solve Eqn. 3 with the user-specified anchors as constraints to determine \mathbf{V}^* .

Taking the derivative with respect to \mathbf{V} , the problem in Eqn. 3 turns into a system of equations

$$(\mathbf{L}^T \mathbf{L} + \lambda \mathbf{K}_a^T \mathbf{K}_a) \mathbf{V} = \mathbf{L}^T \nabla^T \mathcal{A}\mathbf{J} + \lambda \mathbf{K}_a^T \mathbf{T}_a, \quad (4)$$

which can be efficiently solved using a differentiable solver [2] implementing Cholesky decomposition.

We let g denote a functional representing the aforementioned differentiable solver for notational convenience, $\mathbf{V}^* = g(\mathbf{J}, \mathbf{K}_a, \mathbf{T}_a)$. Since g is differentiable, we can deform \mathcal{M}_0 by propagating upstream gradients from various loss functions to the underlying parameterization \mathbf{J} . For instance, one may impose a *soft* constraint on the locations of selected handles during optimization with the objective of the form:

$$\mathcal{L}_h = \|\mathbf{K}_h \mathbf{V}^* - \mathbf{T}_h\|^2. \quad (5)$$

We will discuss how such a soft constraint can be blended into our framework in Sec. 3.3. Next, we describe how to incorporate a pretrained diffusion model as a prior for visual plausibility.

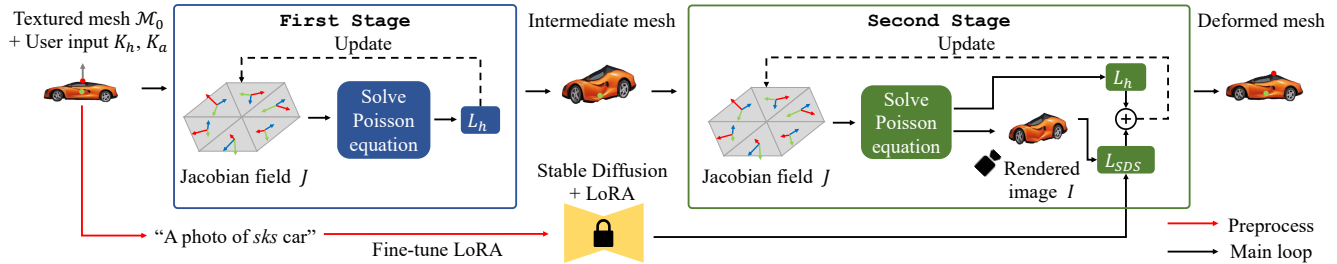


Figure 2. The overview of APAP. APAP parameterizes a triangular mesh as a per-face Jacobian field that can be updated via gradient-descent. Given a textured mesh and user inputs specifying the handle(s) and anchor(s), our framework initializes a Jacobian field as a trainable parameter. During the first stage, the Jacobian field is updated via iterative optimization of \mathcal{L}_h , a soft constraint that initially deforms the shape according to the user’s instruction. In the following stage, the mesh is rendered using a differentiable renderer \mathcal{R} and the rendered image is provided as an input to a diffusion prior finetuned with LoRA [15] that computes the SDS loss \mathcal{L}_{SDS} . The joint optimization of \mathcal{L}_h and \mathcal{L}_{SDS} improves the visual plausibility of the mesh while conforming to the given edit instruction.

241 3.2. Score Distillation for Shape Deformation

242 While traditional mesh deformation techniques make varia-
243 tions that match the given *geometric* constraints, their lack
244 of consideration on *visual plausibility* results in unrealistic
245 shapes. Motivated by recent success in text-to-3D litera-
246 ture, we harness a powerful 2D diffusion prior [43] in our
247 framework as a critic that directs deformation by scoring the
248 realism of the current shape.

249 Specifically, we distill its prior knowledge via Score Dis-
250 tillation Sampling (SDS) [39]. Let \mathbf{J} denote the current Ja-
251 cobian field and \mathbf{V}^* be the set of vertices computed from \mathbf{J}
252 following the procedure described in Sec. 3.1.

253 We render $\mathcal{M}^* = (\mathbf{V}^*, \mathbf{F})$ from a viewpoint defined by
254 camera extrinsic parameters \mathbf{C} using a differentiable ren-
255 derer \mathcal{R} , producing an image $\mathcal{I} = \mathcal{R}(\mathcal{M}^*, \mathbf{C})$. The diffu-
256 sion prior $\hat{\epsilon}_\phi$ then rates the realism of \mathcal{I} , producing a gradi-
257 ent

$$258 \nabla_{\mathbf{J}} \mathcal{L}_{SDS}(\phi, \mathcal{I}) = \mathbb{E}_{t, \epsilon} \left[w(t) (\hat{\epsilon}_\phi(\mathbf{z}_t; y, t) - \epsilon) \frac{\partial \mathcal{I}}{\partial \mathbf{J}} \right], \quad (6)$$

259 where $t \sim \mathcal{U}(0, 1)$, $\epsilon \sim \mathcal{N}(\mathbf{0}, \mathbf{I})$, and \mathbf{z}_t is a noisy latent
260 embedding of \mathcal{I} . The propagated gradient alters the geom-
261 etry of \mathcal{M} by modifying \mathbf{J} .

262 To increase the instance-awareness of the diffusion
263 model, we follow recent work [44, 48] on personalized im-
264 age editing and finetune the model using LoRA [15]. In
265 particular, we first render \mathcal{M} from n different viewpoints
266 to obtain a set $\mathcal{I} = \{\mathcal{I}_1, \dots, \mathcal{I}_n\}$ of training images and
267 inject additional parameters to the model, resulting in an
268 expanded set of network parameters ϕ' . The parameters are
269 then optimized with a denoising loss [43]

$$270 \mathcal{L} = \mathbb{E}_{t, \epsilon, \mathbf{z}} [\|\hat{\epsilon}_{\phi'}(\mathbf{z}_t; y, t) - \epsilon\|^2], \quad (7)$$

271 where \mathbf{z}_t denotes a latent of a training image perturbed with
272 noise at timestep t .

273 The finetuned diffusion prior, together with a learnable
274 Jacobian field representation of the source mesh \mathcal{M}_0 , com-

275 prises the proposed framework described in the following
276 section.

277 3.3. As-Plausible-As-Possible (APAP)

278 **APAP** tackles the problem of plausibility-aware shape de-
279 formation by harmonizing the best of both worlds: a learn-
280 able shape representation founded on classical geometry
281 processing, robust to noisy gradients, and a powerful 2D
282 diffusion prior finetuned with the image(s) of the source
283 mesh for better instance-awareness.

284 We provide an overview of the proposed pipeline in
285 Fig. 2 and the algorithm in Alg. 1. We will delve into details
286 in the following. Provided with a textured mesh \mathcal{M}_0 , han-
287 dles \mathbf{K}_h , anchors \mathbf{K}_a , as well as their target positions \mathbf{T}_h
288 and \mathbf{T}_a as inputs, **APAP** yields a plausible deformation \mathcal{M}
289 of \mathcal{M}_0 that conforms to the given handle-target constraints.
290 Before deforming \mathcal{M}_0 , we render \mathcal{M}_0 from a single view in
291 the case of 2D meshes and four canonical views (i.e., front,
292 back, left, and right) for 3D meshes and use the images to
293 finetune Stable Diffusion [43] by optimizing LoRA [15] pa-
294 rameters injected to the model (the red line in Fig. 2). Si-
295 multaneously, **APAP** computes the Jacobian field \mathbf{J}_0 of the
296 input mesh \mathcal{M}_0 and initializes it as a trainable parameter \mathbf{J} .

297 **APAP** deforms the input mesh through two stages. In the
298 *FirstStage*, it first deforms the input mesh according to
299 instructions from users without taking visual plausibility
300 into account. The subsequent *SecondStage* integrates
301 a 2D diffusion prior into the optimization loop, simultane-
302 ously enforcing user constraints and visual plausibility.

303 At every iteration of the *FirstStage* illustrated as
304 the blue box in Fig. 2, we compute the vertex positions
305 \mathbf{V}^* corresponding to the current Jacobian field \mathbf{J} by solv-
306 ing Eqn. 3 using the anchors specified by \mathbf{K}_a as hard con-
307 straints. Then, we compute the soft constraint \mathcal{L}_h defined as
308 Eqn. 5 that drags a set of handle vertices $\mathbf{K}_h \mathbf{V}^*$ toward
309 the corresponding targets \mathbf{T}_h . The interleaving of differentiable
310 Poisson solve and optimization of \mathcal{L}_h via gradient-descent

Algorithm 1 As-Plausible-As-Possible

Parameters: $g, \mathcal{R}, \phi, \gamma, M, N$
Inputs: $\mathcal{M}_0 = (\mathbf{V}_0, \mathbf{F}_0), \mathbf{K}_a, \mathbf{K}_h, \mathbf{T}_a, \mathbf{T}_h, \{\mathbf{C}_i\}_{i=1}^n$
Output: \mathcal{M}

procedure FIRSTSTAGE($\mathbf{J}, \mathbf{K}_a, \mathbf{K}_h, \mathbf{T}_a, \mathbf{T}_h, g$)
 for $i = 1, 2, \dots, M$ **do**
 $\mathbf{V}^* \leftarrow g(\mathbf{J}, \mathbf{K}_a, \mathbf{T}_a)$ ▷ Solving Eqn. 4
 $\mathbf{J} \leftarrow \mathbf{J} - \gamma \nabla_{\mathbf{J}} \mathcal{L}_h(\mathbf{V}^*, \mathbf{K}_h, \mathbf{T}_h)$
 end for
 return \mathbf{J}
end procedure

procedure SECONDSTAGE($\mathbf{J}, \mathbf{F}_0, \mathbf{K}_a, \mathbf{K}_h, \mathbf{T}_a, \mathbf{T}_h, g, \phi, \{\mathbf{C}_i\}$)
 for $i = 1, 2, \dots, N$ **do**
 $\mathbf{V}^* \leftarrow g(\mathbf{J}, \mathbf{K}_a, \mathbf{T}_a)$ ▷ Solving Eqn. 4
 $\mathcal{M}^* \leftarrow (\mathbf{V}^*, \mathbf{F}_0)$
 $\mathbf{C} \sim \mathcal{U}(\{\mathbf{C}_i\})$ ▷ Viewpoint Sampling
 $\mathcal{I} \leftarrow \mathcal{R}(\mathcal{M}^*, \mathbf{C})$ ▷ Rendering
 $\mathbf{J} \leftarrow \mathbf{J} - \gamma \nabla_{\mathbf{J}} (\mathcal{L}_{\text{SDS}}(\phi, \mathcal{I}) + \mathcal{L}_h(\mathbf{V}^*, \mathbf{K}_h, \mathbf{T}_h))$
 end for
 return \mathbf{J}
end procedure

$\phi \leftarrow \text{LORA}(\phi, \mathcal{M}_0, \mathcal{R}, \{\mathbf{C}_i\})$
 $\mathbf{J} \leftarrow \{\mathbf{J}_{0,f} | f \in \mathbf{F}_0\}$
 $\mathbf{J} \leftarrow \text{FIRSTSTAGE}(\mathbf{J}, \mathbf{K}_a, \mathbf{K}_h, \mathbf{T}_a, \mathbf{T}_h, g)$
 $\mathbf{J} \leftarrow \text{SECONDSTAGE}(\mathbf{J}, \mathbf{F}_0, \mathbf{K}_a, \mathbf{K}_h, \mathbf{T}_a, \mathbf{T}_h, g, \phi, \{\mathbf{C}_i\})$
 $\mathbf{V} \leftarrow g(\mathbf{J}, \mathbf{K}_a, \mathbf{T}_a)$
 $\mathcal{M} \leftarrow (\mathbf{V}, \mathbf{F}_0)$
return \mathcal{M}

311 is repeated for M iterations. This progressively updates \mathbf{J} ,
312 treated as a learnable black box in our framework, deform-
313 ing \mathcal{M}_0 . Consequently, the edited mesh $\mathcal{M}^* = (\mathbf{J}, \mathbf{F}_0)$ fol-
314 lows user constraints at the cost of the degraded plausibility,
315 mitigated in the following stage through the incorporation
316 of a diffusion prior.

317 The result of `FirstStage` then serves as an initializa-
318 tion for the `SecondStage`, illustrated as the *green* box in
319 Fig. 2 guided by plausibility constraint \mathcal{L}_{SDS} . Unlike the
320 `FirstStage` where the update of \mathbf{J} was purely driven
321 by the geometric constraint \mathcal{L}_h , we aim to steer the op-
322 timization based on the visual plausibility of the current
323 mesh \mathcal{M}^* . To achieve this, we render \mathcal{M}^* using a differen-
324 tiable renderer \mathcal{R} using the same viewpoint(s) from which
325 the training image(s) for finetuning was rendered. When
326 deforming 3D meshes, we randomly sample one viewpoint
327 at each iteration. The rendered image \mathcal{I} is used to evaluate
328 \mathcal{L}_{SDS} which is optimized jointly with \mathcal{L}_h for N iterations.
329 The combination of geometric and plausibility constraints

improves the visual plausibility of the output while encour- 330
aging it to conform to the given constraints. 331

We note that the iterative approach in the `FirstStage` 332
leads to better results than alternative update strategies such 333
as deforming the source mesh \mathcal{M}_0 by minimizing ARAP 334
energy [50] or, solving Eqn. 3 using both \mathbf{K}_h and \mathbf{K}_a as 335
hard constraints. In our experiments (Sec. 4), we show that 336
both methods produce distortions that cannot be corrected 337
by the diffusion prior in the subsequent stage. Specifically, 338
directly solving Eqn. 3 using all available constraints only 339
yields the least squares solution \mathbf{V}^* without updating the 340
underlying Jacobians \mathbf{J} , resulting in the aforementioned dis- 341
tortions. 342

4. Experiments 343

We evaluate **APAP** in downstream applications involving 344
manipulation of 3D and 2D meshes. 345

4.1. Experiment Setup 346

Benchmark. To evaluate the plausibility of a mesh de- 347
formation we propose a novel benchmark APAP-BENCH 348
of textured 3D and 2D triangular meshes spanning both 349
human-made and organic objects annotated with handle ver- 350
tices and their editing directions, and anchor vertices. The 351
set of 3D meshes, APAP-BENCH 3D, is constructed using 352
meshes from ShapeNet [6] and *Genie* [1]. The meshes are 353
normalized to fit in a unit cube. Each mesh is manually an- 354
notated with editing instructions, including a set of anchors, 355
handles, and corresponding targets to simulate editing sce- 356
narios. APAP-BENCH offers another subset called APAP- 357
BENCH 2D, a collection of 80 textured, planar meshes of 358
various objects, to facilitate quantitative analysis and user 359
study described later in this section. To create APAP- 360
BENCH 2D, we first generate 2 images of real-world ob- 361
jects for each of the 20 categories using Stable Diffusion- 362
XL [38]. We then extract foreground masks from the gen- 363
erated images using SAM [28] and sample pixels that lie on 364
the boundary and interior. The sampled pixels are used for 365
Delaunay triangulation, constrained with the edges along 366
the main contour of the masks, that produces 2D triangular 367
meshes with texture. We assign two handle and anchor pairs 368
to each mesh that imitate user instructions. For evaluation 369
purposes, we populate the reference set by sampling 1,000 370
images for each object category using Stable Diffusion-XL. 371
The generated images are used to evaluate a perceptual met- 372
ric to assess the plausibility of 2D mesh editing results as 373
described in Sec. 4.3. 374

Baselines. We compare our method (**APAP**) and As- 375
Rigid-As-Possible (ARAP) [50] since it is one of the widely 376
used mesh deformation techniques that permits shape ma- 377
nipulation via direct vertex displacement. Throughout the 378



Figure 3. Qualitative results from 3D shape deformation. We visualize the source shapes and their deformations made using ARAP [50] and ours by following the instructions each of which specifies a handle (red), an edit direction denoted with an arrow (gray), and an anchor (green). We showcase the rendered images captured from two different viewpoints, as well as one zoom-in view highlighting local details.

379 experiments, we use the implementation in libigl [19]
380 with default parameters.

381 **Evaluation Metrics.** In 2D experiments, we conduct
382 quantitative analysis based on k -NN GIQA score [12] as
383 an evaluation metric to assess the plausibility of instance-
384 specific editing results. The metric quantifies the perceptual
385 proximity between the edited image and its k nearest neigh-

386 bors in the reference set included in APAP-BENCH 2D. As
387 our objective is to make plausible variations of 2D meshes
388 via deformation, an edited object should remain perceptually
389 similar to other objects in the same category. We use
390 $k = 12$ throughout the experiments.

4.2. 3D Shape Deformation 391

392 **Qualitative Results.** We showcase examples of 3D shape
393 deformation where each deformation is specified by a han-



Figure 4. Failure cases of DragDiffusion. DragDiffusion [48] can easily compromise the identity of edited instances as it manipulates their latents without an explicit parameterization, the identity of instances can be broken during editing.

394 dle (*red*), an edit direction (*gray*), and an anchor (*green*).
 395 As shown in Fig. 3, **APAP** is capable of manipulating
 396 3D shapes to improve visual plausibility which is not
 397 achievable by solely relying on geometric prior such as
 398 ARAP [50]. For instance, given a user input that drags
 399 a handle on one blade of an axe (the first row) along an
 400 arrow, **APAP** simultaneously expands both blades of the
 401 axe whereas ARAP [50] produces distortions near the head.
 402 Similar examples that demonstrate symmetry-awareness of
 403 **APAP** can be found in other cases such as a car (the sec-
 404 ond row), and an owl (the sixth row) where a user lifts only
 405 one side of the shape upward and the symmetry is recovered
 406 by **APAP** which cannot be achieved by ARAP [50]. Also,
 407 note that **APAP** is capable of making a smooth articulation
 408 at the leg of the wolf (the fourth row) by adjusting the over-
 409 all posture in comparison to ARAP which creates an excess
 410 bending.

411 4.3. 2D Mesh Editing

412 **Qualitative Evaluation.** We present qualitative results
 413 using the baselines and our method in Fig. 5. Each row
 414 shows two different results obtained by editing an image
 415 based on a handle moved from the original position (*red*)
 416 along a direction indicated by an arrow (*gray*) while fixing
 417 an anchor (*green*), similar to the 3D experiments discussed
 418 in the previous section.

419 As shown in Fig. 5, ARAP [50] enforces local rigidity
 420 and often results in implausible deformations. For example,
 421 it does not account for the mechanics of the human body
 422 and introduces an unrealistic articulation of a human arm
 423 (the fourth row). In addition, it twists the body of a sports
 424 car (the fifth row). Both of them originate from the lack
 425 of understanding of the appearance of objects. **APAP** alle-
 426 viates this issue by incorporating a visual prior into shape

Methods	k -NN GIQA ($\times 10^{-2}$) \uparrow
ARAP [50]	4.753
DragDiffusion [48]	4.545
Ours (\mathcal{L}_h Only)	4.797
Ours (ARAP Init.)	4.740
Ours (Poisson Init.)	4.316
Ours	4.887

Table 1. Quantitative analysis for 2D mesh editing. APAP outperforms its baselines in quantitative evaluation using k -NN GIQA [12].

Methods	Preference (%) \uparrow
ARAP [50]	40.83
Ours	59.17

Table 2. User study preference for 2D image editing. In a user study targeting users on Amazon Mechanical Turk (MTurk), the results produced using ours were preferred over the outputs from the baseline.

deformation producing a bending near the elbow and pre- 427
 serving the smooth silhouette of the car, respectively. 428

While **APAP** is designed for meshes not images, we pro- 429
 vide an additional qualitative comparison against DragDif- 430
 fusion [48], an image editing technique that operates in 431
 pixel space, to demonstrate the effectiveness of mesh-based 432
 parameterization in applications where identity preservation 433
 is crucial. As shown in Fig. 4, DragDiffusion [48] may cor- 434
 rupt the identity of the instances depicted in input images 435
 during the encoding and decoding procedure. **APAP**, on 436
 the other hand, makes plausible variations of the given ob- 437
 jects while maintaining their originality, benefiting from an 438
 explicit mesh representation it is grounded. 439

Quantitative Evaluation. Tab. 1 summarizes k -NN 440
 GIQA scores measured on the outputs from ARAP [50] (the 441
 first row) and **APAP** (the sixth row) using APAP-BENCH 442
 2D. As shown, **APAP** demonstrates superior performance 443
 over ARAP [50]. This again verifies the observations from 444
 qualitative evaluation where ARAP [50] introduces distor- 445
 tions that harm visual plausibility. As in qualitative eval- 446
 uation, we also report the k -NN GIQA score of DragDif- 447
 fusion [48], degraded due to artifacts caused during direct 448
 manipulation of latents. 449

User Study. We further conduct a user study for a more 450
 precise perceptual analysis. We follow Ritchie [42] and 451
 recruit participants on Amazon Mechanical Turk (MTurk). 452
 Each participant is provided with a set of 20 randomly sam- 453
 pled images of the source meshes paired with editing results 454
 of ARAP [50] and **APAP**. To check whether the response 455
 from a participant is reliable we present 5 vigilance tests 456
 and collect 102 responses from the participants who passed 457

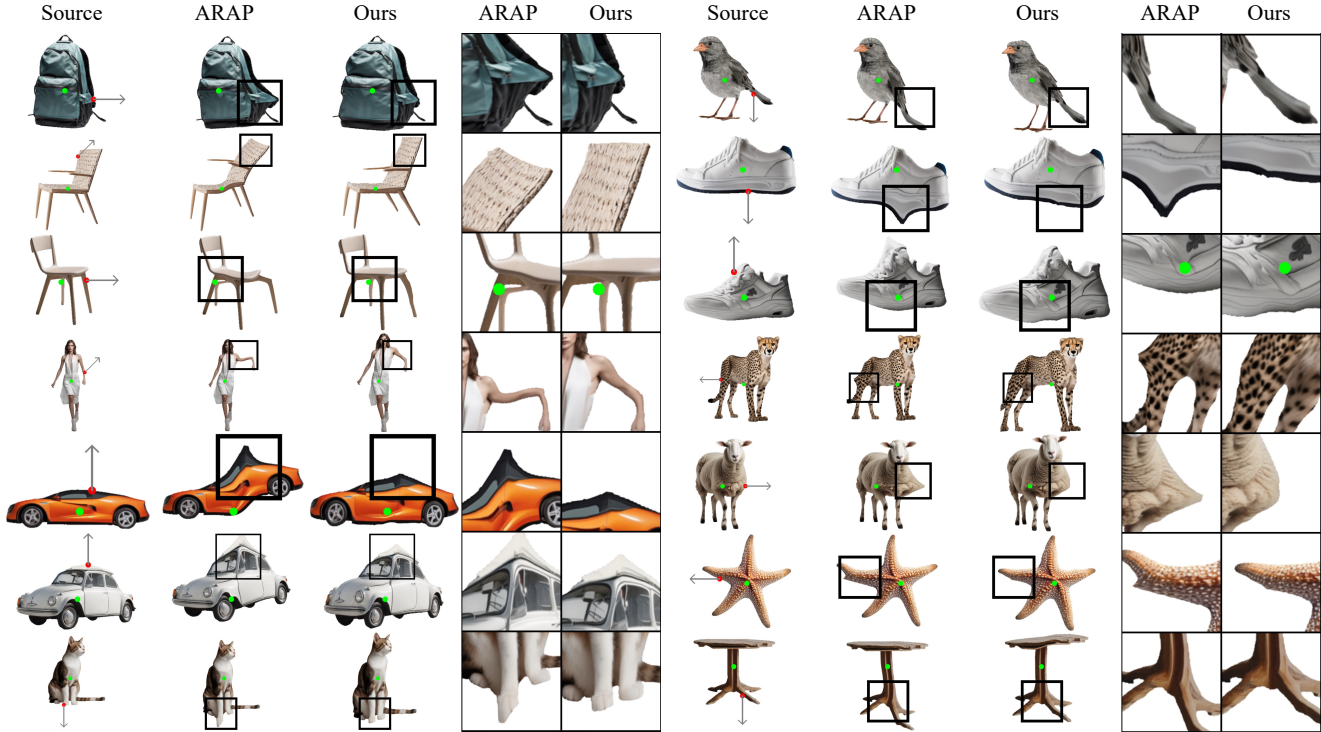


Figure 5. Qualitative results from 2D mesh deformation. 2D meshes are edited using ARAP [50] and the proposed method following the edit instruction consisting of a handle (red), a target direction (gray), and an anchor (green). We showcase the rendered images of the edited meshes, as well as a zoom-in view highlighting local details.

458 the vigilance test.

459 We instructed participants to select the most anticipated
460 outcome when the displayed source image is edited by the
461 dragging operation visualized as an arrow. We have provided
462 detailed settings and examples of the user study environment
463 and statistical methods in the **supplementary material**.
464 Tab. 2 shows a higher preference of the participants
465 on our method over ARAP [50] implying that our method
466 produces more visually plausible deformations by utilizing
467 a visual prior.

468 **Ablation Study.** Tab. 1 summarizes the impact of different
469 initialization strategies in the first stage on k -NN GIQA
470 score. As reported in the third row of the table, optimizing
471 \mathcal{L}_h that aims to exclusively satisfy geometric constraints
472 leads to unnatural distortions. We provide a qualitative
473 comparison in the the **supplementary material**.

474 While designing the algorithm illustrated in Alg. 1, we
475 considered other options for `FirstStage`. Instead of optimizing
476 \mathcal{L}_h to initially deform a shape, we used a shape produced
477 by ARAP [50] or by solving a Poisson’s equation constrained
478 not only on anchor positions but also on handles at their
479 target positions reached by following the given edit directions.
480 We report k -NN GIQA scores of the alternatives in the fourth
481 and fifth row of Tab. 1, respectively. Both ini-

482 tialization strategies degrade the plausibility of results due
483 to large distortions introduced by either solely enforcing local
484 rigidity or, finding least square solutions without updating
485 Jacobians. This poses a challenge to the diffusion prior,
486 making it struggle to induce meaningful update directions
487 when provided with renderings with noticeable distortions,
488 which can be found in qualitative analysis in the **supple-**
489 **mentary material**.

5. Conclusion 490

491 We presented **APAP**, a novel deformation framework that
492 tackles the problem of plausibility-aware shape deformation
493 while offering intuitive controls over a wide range of shapes
494 represented as triangular meshes. To this end, we carefully
495 orchestrate two core components, a learnable Jacobian-based
496 parameterization that originates from geometry processing
497 and powerful 2D priors acquired by text-to-image diffusion
498 models trained on Internet-scale datasets. We assessed the
499 performance of the proposed method against an existing
500 geometric-prior-based deformation technique and also
501 thoroughly investigated the significance of our design
502 choices through experiments.

References

- 503
- 504 [1] Luma AI. Genie. 5 562
- 505 [2] Noam Aigerman, Kunal Gupta, Vladimir G Kim, Siddhartha 563
- 506 Chaudhuri, Jun Saito, and Thibault Groueix. Neural Ja- 564
- 507 cobian Fields: Learning Intrinsic Mappings of Arbitrary 565
- 508 Meshes. *ACM TOG*, 2022. 2, 3 566
- 509 [3] Omer Bar-Tal, Lior Yariv, Yaron Lipman, and Tali Dekel. 567
- 510 MultiDiffusion: Fusing Diffusion Paths for Controlled Im- 568
- 511 age Generation. In *ICML*, 2023. 3 569
- 512 [4] Ilya Baran and Jovan Popović. Automatic Rigging and Ani- 570
- 513 mation of 3D Characters. *ACM TOG*, 2007. 2 571
- 514 [5] Mingdeng Cao, Xintao Wang, Zhongang Qi, Ying Shan, Xi- 572
- 515 aohu Qie, and Yinqiang Zheng. MasaCtrl: Tuning-Free Mu- 573
- 516 tual Self-Attention Control for Consistent Image Synthesis 574
- 517 and Editing. In *ICCV*, 2023. 3 575
- 518 [6] Angel X Chang, Thomas Funkhouser, Leonidas Guibas, Pat 576
- 519 Hanrahan, Qixing Huang, Zimo Li, Silvio Savarese, Manolis 577
- 520 Savva, Shuran Song, Hao Su, et al. ShapeNet: An 578
- 521 Information-Rich 3D Model Repository. *arXiv preprint* 579
- 522 *arXiv:1512.03012*, 2015. 2, 5 580
- 523 [7] Matt Deitke, Ruoshi Liu, Matthew Wallingford, Huong Ngo, 581
- 524 Oscar Michel, Aditya Kusupati, Alan Fan, Christian Laforte, 582
- 525 Vikram Voleti, Samir Yitzhak Gadre, Eli VanderBilt, Anirudha 583
- 526 Kembhavi, Carl Vondrick, Georgia Gkioxari, Kiana 584
- 527 Ehsani, Ludwig Schmidt, and Ali Farhadi. Objaverse-XL: 585
- 528 A Universe of 10M+ 3D Objects. In *NeurIPS*, 2023. 586
- 529 [8] Matt Deitke, Dustin Schwenk, Jordi Salvador, Luca Weihs, 587
- 530 Oscar Michel, Eli VanderBilt, Ludwig Schmidt, Kiana 588
- 531 Ehsani, Aniruddha Kembhavi, and Ali Farhadi. Objaverse: 589
- 532 A Universe of Annotated 3D Objects. In *CVPR*, 2023. 2 590
- 533 [9] Hugging Face. DreamBooth fine-tuning with LoRA. 591
- 534 [10] Rinon Gal, Yuval Alaluf, Yuval Atzmon, Or Patashnik, 592
- 535 Amit H. Bermano, Gal Chechik, and Daniel Cohen-Or. An 593
- 536 Image is Worth One Word: Personalizing Text-to-Image 594
- 537 Generation using Textual Inversion. In *ICLR*, 2023. 3 595
- 538 [11] William Gao, Noam Aigerman, Groueix Thibault, Vladimir 596
- 539 Kim, and Rana Hanocka. TextDeformer: Geometry Manip- 597
- 540 ulation using Text Guidance. *ACM TOG*, 2023. 2, 3 598
- 541 [12] Shuyang Gu, Jianmin Bao, Dong Chen, and Fang Wen. 599
- 542 GIQA: Generated Image Quality Assessment. In *ECCV*, 600
- 543 2020. 2, 6, 7 601
- 544 [13] Amir Hertz, Kfir Aberman, and Daniel Cohen-Or. Delta De- 602
- 545 noising Score. In *ICCV*, 2023. 3 603
- 546 [14] Amir Hertz, Ron Mokady, Jay Tenenbaum, Kfir Aberman, 604
- 547 Yael Pritch, and Daniel Cohen-Or. Prompt-to-Prompt Image 605
- 548 Editing with Cross-Attention Control. In *ICLR*, 2023. 3 606
- 549 [15] Yelong Hu, Edward J. and Shen, Phillip Wallis, Zeyuan 607
- 550 Allen-Zhu, Yuanzhi Li, Shean Wang, and Weizhu Chen. 608
- 551 LoRA: Low-Rank Adaptation of Large Language Models. 609
- 552 In *ICLR*, 2022. 3, 4 610
- 553 [16] Takeo Igarashi, Tomer Moscovich, and John F. Hughes. As- 611
- 554 Rigid-as-Possible Shape Manipulation. *ACM TOG*, 2005. 2 612
- 555 [17] Shir Iluz, Yael Vinker, Amir Hertz, Daniel Berio, Daniel 613
- 556 Cohen-Or, and Ariel Shamir. Word-As-Image for Semantic 614
- 557 Typography. *ACM TOG*, 2023. 2 615
- 558 [18] Alec Jacobson, Ilya Baran, Jovan Popović, and Olga Sorkine. 616
- 559 Bounded Biharmonic Weights for Real-Time Deformation. 617
- 560 *ACM TOG*, 2011. 2 618
- 561 [19] Alec Jacobson, Daniele Panozzo, et al. libigl: A simple C++ 619
- geometry processing library, 2018. 6 620
- [20] Ajay Jain, Amber Xie, and Pieter Abbeel. VectorFusion: 621
- Text-to-SVG by Abstracting Pixel-Based Diffusion Models. 622
- In *CVPR*, 2023. 2 623
- [21] Tomas Jakab, Richard Tucker, Ameesh Makadia, Jiajun Wu, 624
- Noah Snively, and Angjoo Kanazawa. KeypointDeformer: 625
- Unsupervised 3D Keypoint Discovery for Shape Control. In 626
- CVPR*, 2020. 2 627
- [22] Jong Chul Ye Jangho Park, Gihyun Kwon. ED-NeRF: Effi- 628
- cient Text-Guided Editing of 3D Scene using Latent Space 629
- NeRF. *arXiv*, 2023. 2 630
- [23] Pushkar Joshi, Mark Meyer, Tony DeRose, Brian Green, and 631
- Tom Sanocki. Harmonic Coordinates for Character Articulation. 632
- ACM TOG*, 2007. 2 633
- [24] Tao Ju, Scott Schaefer, and Joe Warren. Mean Value Co- 634
- ordinates for Closed Triangular Meshes. *ACM TOG*, 2005. 635
- 2 636
- [25] Nasir Mohammad Khalid, Tianhao Xie, Eugene Belilovsky, 637
- and Popa Tiberiu. CLIP-Mesh: Generating Textured Meshes 638
- from Text Using Pretrained Image-Text Models. *SIGGRAPH* 639
- ASIA*, 2022. 3 640
- [26] Kunho Kim, Mikaela Angelina Uy, Despoina Paschalidou, 641
- Alec Jacobson, Leonidas J. Guibas, and Minhyuk Sung. 642
- OptCtrlPoints: Finding the Optimal Control Points for Bi- 643
- harmonic 3D Shape Deformation. *Computer Graphics For- 644*
- um*, 2023. 2 645
- [27] Subin Kim, Kyungmin Lee, June Suk Choi, Jongheon Jeong, 646
- Kihyuk Sohn, and Jinwoo Shin. Collaborative Score Distil- 647
- lation for Consistent Visual Synthesis. In *NeurIPS*, 2023. 2 648
- [28] Alexander Kirillov, Eric Mintun, Nikhila Ravi, Hanzi Mao, 649
- Chloe Rolland, Laura Gustafson, Tete Xiao, Spencer White- 650
- head, Alexander C. Berg, Wan-Yen Lo, Piotr Dollár, and 651
- Ross Girshick. Segment Anything. In *ICCV*, 2023. 5 652
- [29] Juil Koo, Seungwoo Yoo, Minh Hieu Nguyen, and Minhyuk 653
- Sung. SALAD: Part-Level Latent Diffusion for 3D Shape 654
- Generation and Manipulation. In *ICCV*, 2023. 1 655
- [30] Yuseung Lee, Kunho Kim, Hyunjin Kim, and Minhyuk 656
- Sung. SyncDiffusion: Coherent Montage via Synchronized 657
- Joint Diffusions. In *NeurIPS*, 2023. 3 658
- [31] Yaron Lipman, David Levin, and Daniel Cohen-Or. Green 659
- Coordinates. *ACM TOG*, 2008. 2 660
- [32] Yaron Lipman, Olga Sorkine, Daniel Cohen-Or, David 661
- Levin, Christian Rössl, and Hans-Peter Seidel. Differential 662
- Coordinates for Interactive Mesh Editing. In *Proceedings of* 663
- Shape Modeling International*, pages 181–190, 2004. 2 664
- [33] Yaron Lipman, Olga Sorkine, David Levin, and Daniel 665
- Cohen-Or. Linear Rotation-Invariant Coordinates for 666
- Meshes. *ACM TOG*, 2005. 2 667
- [34] Minghua Liu, Minhyuk Sung, Radomir Mech, and Hao Su. 668
- DeepMetaHandles: Learning Deformation Meta-Handles of 669
- 3D Meshes with Biharmonic Coordinates. In *CVPR*, 2021. 670
- 2 671
- [35] Yuan Liu, Cheng Lin, Zijiao Zeng, Xiaoxiao Long, Lingjie 672
- Liu, Taku Komura, and Wenping Wang. SyncDreamer: 673
- Learning to Generate Multiview-consistent Images from a 674
- Single-view Image. *arXiv*, 2023. 1, 3 675
- [36] Oscar Michel, Roi Bar-On, Richard Liu, Sagie Benaim, and 676
- Rana Hanocka. Text2Mesh: Text-Driven Neural Stylization 677
- for Meshes. In *CVPR*, 2022. 3 678
- [37] Xingang Pan, Ayush Tewari, Thomas Leimkühler, Lingjie 679

- 622 Liu, Abhimitra Meka, and Christian Theobalt. Drag Your
623 GAN: Interactive Point-based Manipulation on the Genera-
624 tive Image Manifold. *ACM TOG*, 2023. 3
- 625 [38] Dustin Podell, Zion English, Kyle Lacey, Andreas
626 Blattmann, Tim Dockhorn, Jonas Müller, Joe Penna, and
627 Robin Rombach. SDXL: Improving Latent Diffusion Mod-
628 els for High-Resolution Image Synthesis. *arXiv*, 2023. 5
- 629 [39] Ben Poole, Ajay Jain, Jonathan T Barron, and Ben Milden-
630 hall. DreamFusion: Text-to-3D using 2D Diffusion. In *ICLR*,
631 2023. 1, 2, 3, 4
- 632 [40] Alec Radford, Jong Wook Kim, Chris Hallacy, Aditya
633 Ramesh, Gabriel Goh, Sandhini Agarwal, Girish Sastry,
634 Amanda Askell, Pamela Mishkin, Jack Clark, et al. Learning
635 Transferable Visual Models from Natural Language Supervi-
636 sion. In *ICML*, 2021. 3
- 637 [41] Amit Raj, Srinivas Kaza, Ben Poole, Michael Niemeyer,
638 Ben Mildenhall, Nataniel Ruiz, Shiran Zada, Kfir Aberman,
639 Michael Rubenstein, Jonathan Barron, Yuanzhen Li, and
640 Varun Jampani. DreamBooth3D: Subject-Driven Text-to-3D
641 Generation. In *ICCV*, 2023. 1
- 642 [42] Daniel Ritchie. Rudimentary framework for running two-
643 alternative forced choice (2afc) perceptual studies on me-
644 chanical turk. 7
- 645 [43] Robin Rombach, Andreas Blattmann, Dominik Lorenz,
646 Patrick Esser, and Björn Ommer. High-Resolution Image
647 Synthesis with Latent Diffusion Models. In *CVPR*, 2022. 3,
648 4
- 649 [44] Nataniel Ruiz, Yuanzhen Li, Varun Jampani, Yael Pritch,
650 Michael Rubinstein, and Kfir Aberman. DreamBooth: Fine
651 Tuning Text-to-image Diffusion Models for Subject-Driven
652 Generation. In *CVPR*, 2023. 3, 4
- 653 [45] Christoph Schuhmann, Romain Beaumont, Richard Vencu,
654 Cade Gordon, Ross Wightman, Mehdi Cherti, Theo
655 Coombes, Aarush Katta, Clayton Mullis, Mitchell Worts-
656 man, Patrick Schramowski, Srivatsa Kundurthy, Katherine
657 Crowson, Ludwig Schmidt, Robert Kaczmarczyk, and Jenia
658 Jitsev. LAION-5B: An open large-scale dataset for training
659 next generation image-text models. In *NeurIPS*, 2022. 3
- 660 [46] Tianchang Shen, Jun Gao, Kangxue Yin, Ming-Yu Liu, and
661 Sanja Fidler. Deep Marching Tetrahedra: a Hybrid Rep-
662 resentation for High-Resolution 3D Shape Synthesis. In
663 *NeurIPS*, 2021. 1
- 664 [47] Yichun Shi, Peng Wang, Jianglong Ye, Long Mai, Kejie Li,
665 and Xiao Yang. MVDream: Multi-view Diffusion for 3D
666 Generation. *arXiv*, 2023. 1, 3
- 667 [48] Yujun Shi, Chuhui Xue, Jiachun Pan, Wenqing Zhang, Vin-
668 cent YF Tan, and Song Bai. DragDiffusion: Harnessing
669 Diffusion Models for Interactive Point-based Image Editing.
670 *arXiv*, 2023. 3, 4, 7
- 671 [49] J. Ryan Shue, Eric Ryan Chan, Ryan Po, Zachary Ankner,
672 Jiajun Wu, and Gordon Wetzstein. 3D Neural Field Genera-
673 tion using Triplane Diffusion. In *CVPR*, 2023. 1
- 674 [50] Olga Sorkine and Marc Alexa. As-Rigid-As-Possible Sur-
675 face Modeling. *Proceedings of EUROGRAPHICS/ACM*
676 *SIGGRAPH Symposium on Geometry Processing*, pages
677 109–116, 2007. 2, 5, 6, 7, 8
- 678 [51] Olga Sorkine, Daniel Cohen-Or, Yaron Lipman, Marc Alexa,
679 Christian Rössl, and Hans-Peter Seidel. Laplacian Surface
680 Editing. *Proceedings of the EUROGRAPHICS/ACM SIG-*
GRAPH Symposium on Geometry Processing, pages 179–
188, 2004. 2
- [52] Jiapeng Tang, Markhasin Lev, Wang Bi, Thies Justus, and
Matthias Nießner. Neural Shape Deformation Priors. In
NeurIPS, 2022. 2
- [53] Jiaxiang Tang, Jiawei Ren, Hang Zhou, Ziwei Liu, and Gang
Zeng. DreamGaussian: Generative Gaussian Splatting for
Efficient 3D Content Creation. *arXiv*, 2023. 1, 3
- [54] Narek Tumanyan, Michal Geyer, Shai Bagon, and Tali
Dekel. Plug-and-Play Diffusion Features for Text-Driven
Image-to-Image Translation. In *CVPR*, 2023. 3
- [55] Yu Wang, Alec Jacobson, Jernej Barbič, and Ladislav Kavan.
Linear Subspace Design for Real-Time Shape Deformation.
ACM TOG, 2015. 2
- [56] Zhengyi Wang, Cheng Lu, Yikai Wang, Fan Bao, Chongxuan
Li, Hang Su, and Jun Zhu. Prolificdreamer: High-fidelity and
diverse text-to-3d generation with variational score distilla-
tion. In *NeurIPS*, 2023. 1, 3
- [57] Ofir Weber, Mirela Ben-Chen, and Craig Gotsman. Complex
barycentric coordinates with applications to planar shape de-
formation. *Computer Graphics Forum*, 2009. 2
- [58] Ofir Weber, Olga Sorkine, Yaron Lipman, and Craig Gots-
man. Context-Aware Skeletal Shape Deformation. *Computer*
Graphics Forum, 2007. 2
- [59] Tong Wu, Jiarui Zhang, Xiao Fu, Yuxin Wang, Jiawei
Ren, Liang Pan, Wayne Wu, Lei Yang, Jiaqi Wang, Chen
Qian, Dahua Lin, and Ziwei Liu. OmniObject3D: Large-
Vocabulary 3D Object Dataset for Realistic Perception, Re-
construction and Generation. In *CVPR*, 2023. 2
- [60] Zhan Xu, Yang Zhou, Evangelos Kalogerakis, Chris Lan-
dreth, and Karan Singh. RigNet: Neural Rigging for Artic-
ulated Characters. *ACM TOG*, 2020. 2
- [61] Zhan Xu, Yang Zhou, Li Yi, and Evangelos Kalogerakis.
Morig: Motion-Aware Rigging of Character Meshes from
Point Clouds. In *SIGGRAPH ASIA*, 2022. 2
- [62] Wang Yifan, Noam Aigerman, Vladimir G. Kim, Chaud-
huri Siddhartha, and Olga Sorkine. Neural Cages for Detail-
Preserving 3D Deformations. In *CVPR*, 2020. 2
- [63] Lvmin Zhang, Anyi Rao, and Maneesh Agrawala. Adding
Conditional Control to Text-to-Image Diffusion Models. In
ICCV, 2023. 3
- [64] Yuechen Zhang, Jinbo Xing, Eric Lo, and Jiaya Jia. Real-
World Image Variation by Aligning Diffusion Inversion
Chain. In *NeurIPS*, 2023. 3
- [65] Jingyu Zhuang, Chen Wang, Lingjie Liu, Liang Lin, and
Guanbin Li. DreamEditor: Text-Driven 3D Scene Editing
with Neural Fields. *ACM TOG*, 2023. 2, 3